# Simulation of transcranial magnetic stimulation in head model with morphologically-realistic cortical neurons

## Supplementary materials

Authors: Aman S. Aberra[a], Boshuo Wang[b], Warren M. Grill[a,c,d,e], Angel V. Peterchev[a,b,c,e*]

[a] Department of Biomedical Engineering, Duke University, Durham, NC 27708

[b] Department of Psychiatry and Behavioral Sciences, Duke University, Durham, NC 27710

[c] Department of Electrical and Computer Engineering, Duke University, Durham, NC 27708

[d] Department of Neurobiology, School of Medicine, Duke University, Durham, NC 27710

[e] Department of Neurosurgery, School of Medicine, Duke University, Durham, NC 27710

Email addresses:
aman.aberra@duke.edu, boshuo.wang@duke.edu, warren.grill@duke.edu, and angel.peterchev@duke.edu

Corresponding author: A.V. Peterchev

Phone: +1 919 684 0383

E-mail: angel.peterchev@duke.edu

Address: Division of Brain Stimulation and Neurophysiology, Department of Psychiatry and Behavioral Sciences, Duke University, Box 3620, DUMC, Durham, NC 27710, USA

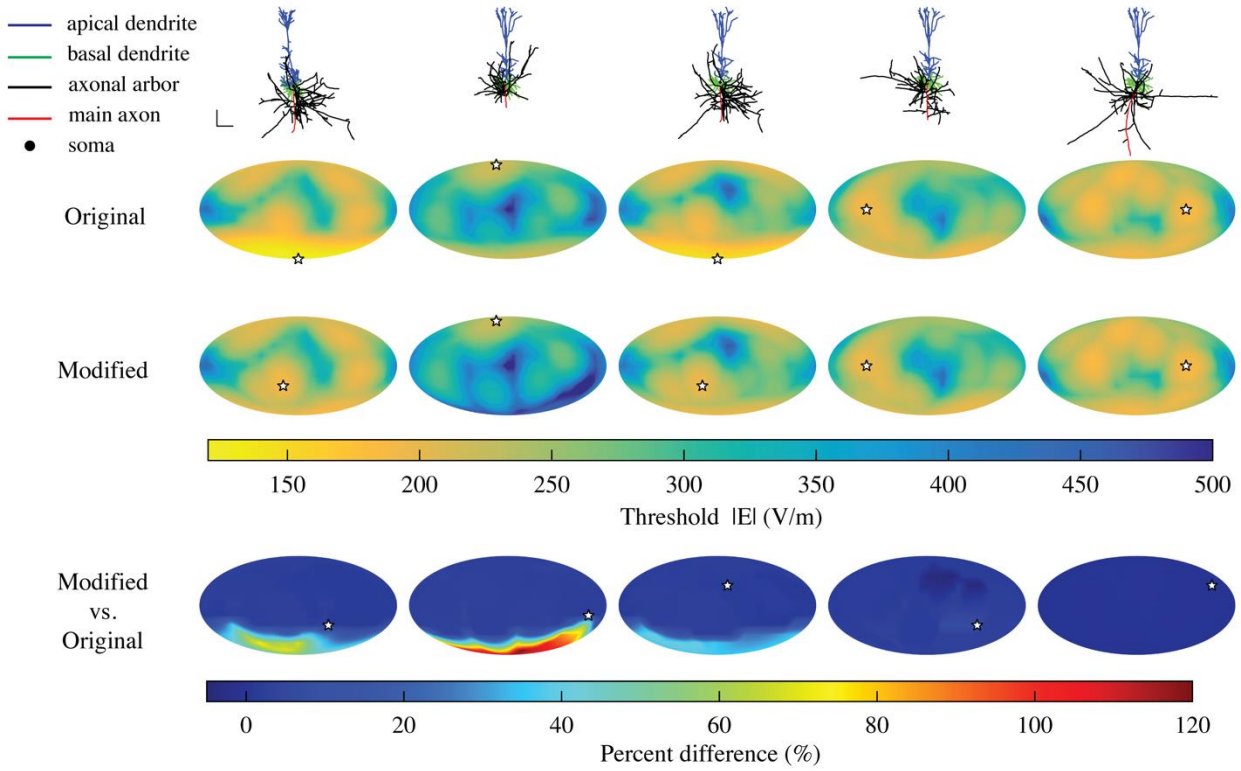


**Supplementary Figure 1. Effect of disabling main axon terminal of L5 pyramidal cells on threshold maps.** The rows depict for each L5 PC clone, from top to bottom: cell morphology, original threshold map with no modification to main axon terminal, threshold map of cell with main axon terminal disabled by setting end compartment diameter to 1000 µm, and map of threshold percent differences between modified cell and original cell for each E-field direction. Notice the significant increase in thresholds for downward E-field directions in cells 1–3 when the main axon terminal is excluded as an activation-capable site.

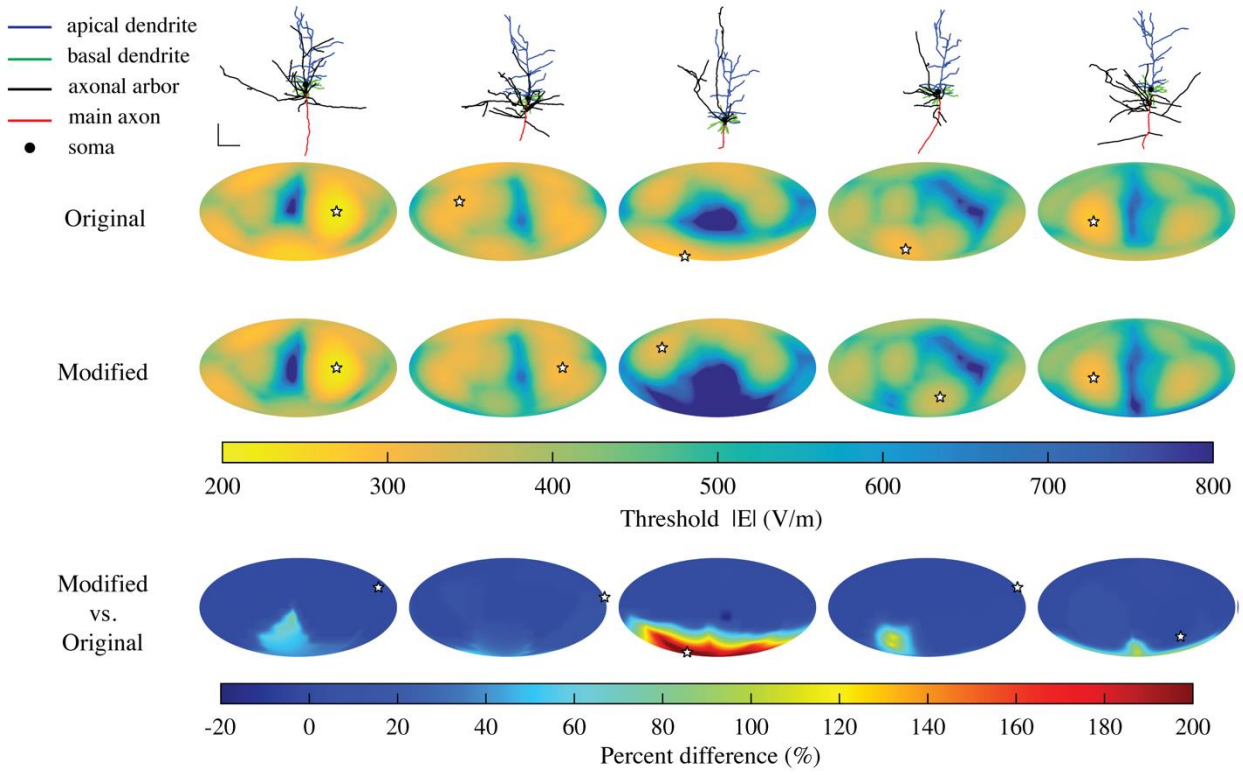


**Supplementary Figure 2. Effect of disabling main axon terminal of L6 pyramidal cells on threshold maps.** Same as Supplementary Figure 1 but for L6 PCs.

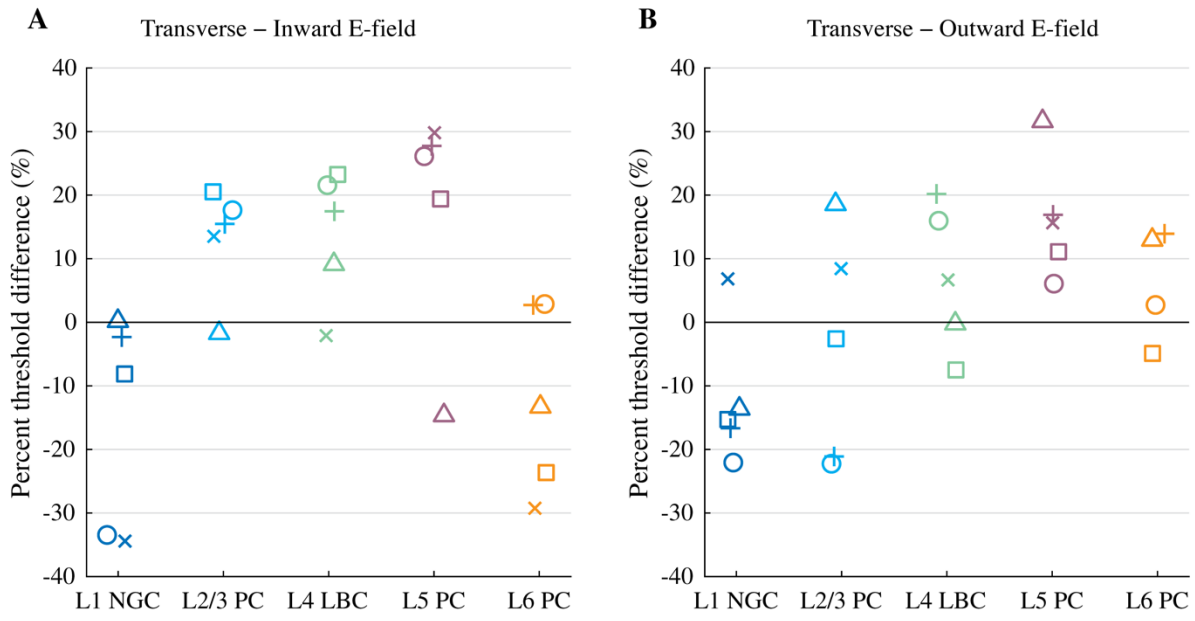


**Supplementary Figure 3. Threshold differences for transverse and inward/outward uniform E-field.** Percent difference in threshold for **A)** transverse versus inward E-field and **B)** transverse versus outward E-field. Average thresholds were computed for E-fields directed transverse ($60° < \theta \leq 120°$) and approximately parallel to the somato-dendritic axis—either upwards, towards the pial surface ($0 \leq \theta \leq 60°$), or downwards, towards the white matter ($120° < \theta \leq 180°$)—after averaging thresholds across all azimuthal rotations within the relevant polar angles. Symbols for each clone match Figure1E.

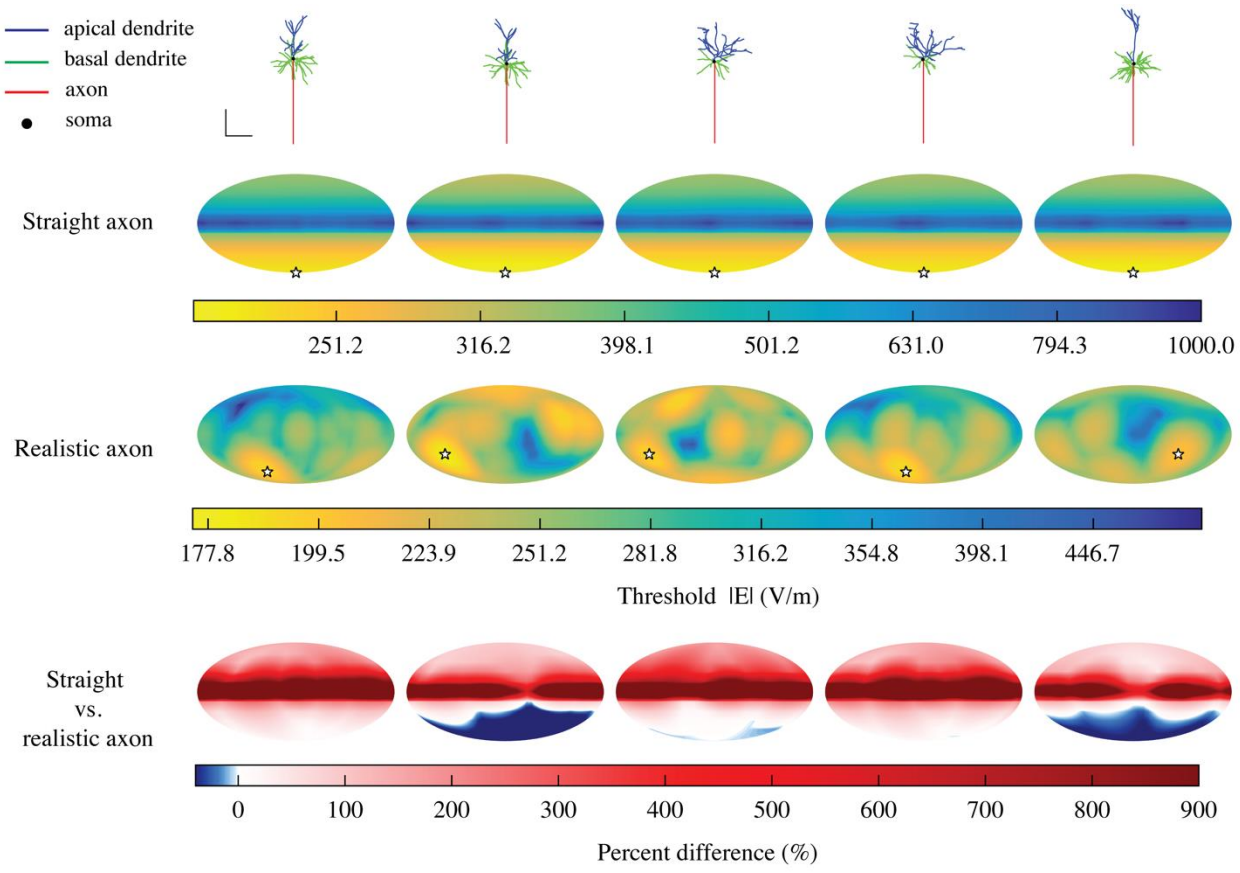


**Supplementary Figure 4. Effect of straight axon morphology of L2/3 pyramidal cells on threshold maps.** The rows depict for each L2/3 PC clone, from top to bottom: cell morphology, threshold map of cell with artificial straight axon, threshold map with realistic axon morphology (same as Figure 1D), and map of threshold percent differences between straight axon and realistic axon for each E-field direction.

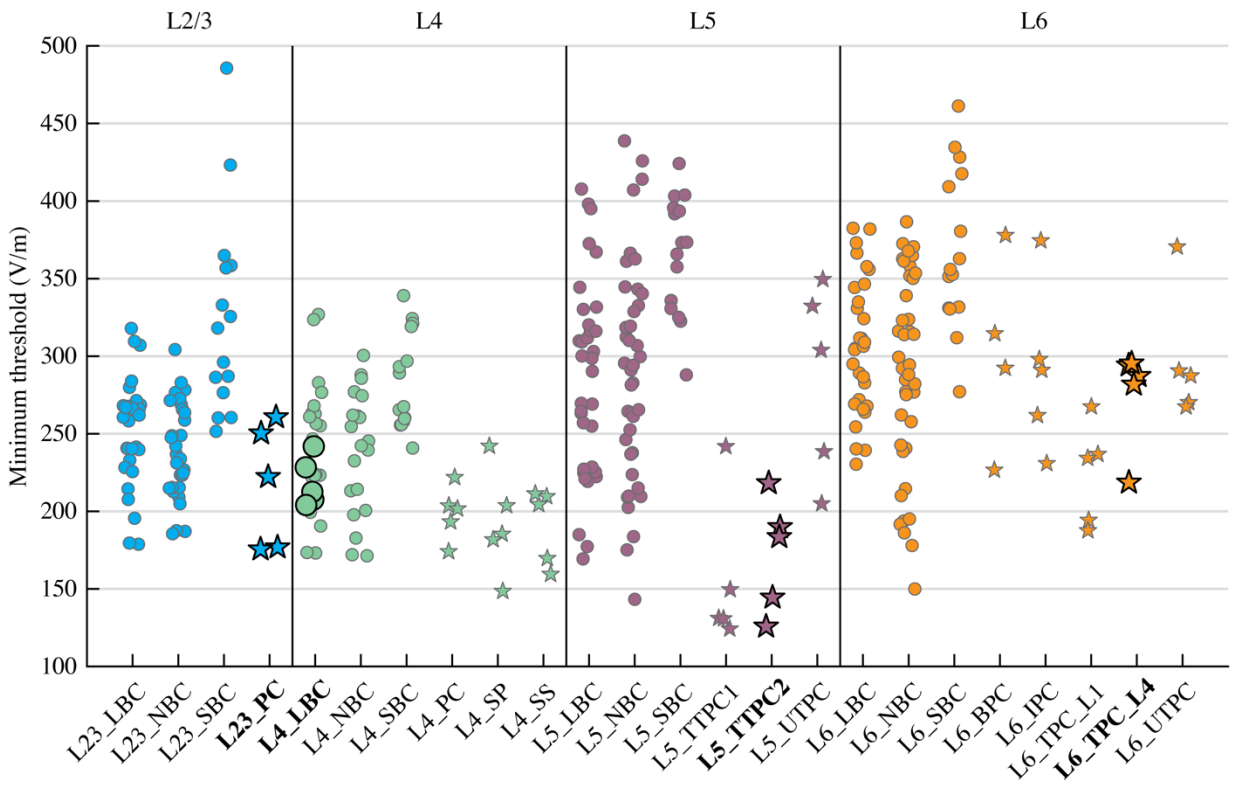


**Supplementary Figure 5. Minimum threshold for all myelinated cortical cell types in the Blue Brain library with uniform E-field.** The minimum threshold was extracted from threshold–direction maps for five virtual clones of all cell types expected to possess some degree of myelination, i.e. inhibitory basket cells and excitatory cells. Inhibitory and excitatory cells are indicated by circle and star symbols, respectively. The thresholds for the model neurons that we previously published [25] and included in the multi-scale model in this paper are shown enlarged with black outlines and bold labels. The inhibitory morphological types have more than five points because they each have multiple electrical types, with five virtual clones per morpho-electrical type. The same methods were used to modify the full library of Blue Brain library model neurons and generate threshold–direction maps, except we used 30° steps for sampling polar and azimuthal directions, giving 62 total thresholds per model neuron from which the minimum was extracted, and we did not disable the main axon terminal of any of the model neurons. Additionally, some model neurons did not have a constant steady state membrane potential, so they were initialized at an approximate rest potential. The rest potential was determined for these models by simulating them for 3 sec with no stimulus and taking the mean membrane potential for the latter 2.5 sec, if the membrane potential exhibited subthreshold oscillations, or taking the final membrane potential value, if the membrane potential exhibited spontaneous firing or monotonic drift. Cell model names consist of layer (L2/3, L4, L5, or L6) and morphological-type, which are abbreviated as follows: large basket cell (LBC), nest basket cell (NBC),

pyramidal cell (PC), small basket cell (SBC), star pyramidal cell (SP), spiny stellate cell (SS), small tufted pyramidal cell (STPC), thick-tufted pyramidal cell with apical trunk that bifurcated at the distal half of the apical dendrite (TTPC1) or proximal half of the apical dendrite (TTPC2), untufted pyramidal cell (UTPC), inverted pyramidal cell (IPC), bipolar pyramidal cell (BPC), and tufted pyramidal cell with apical dendrite terminating in L1 (TPC_L1) or L4 (TPC_L4). Layer 1 cells are not represented because their axons are not expected to be myelinated.

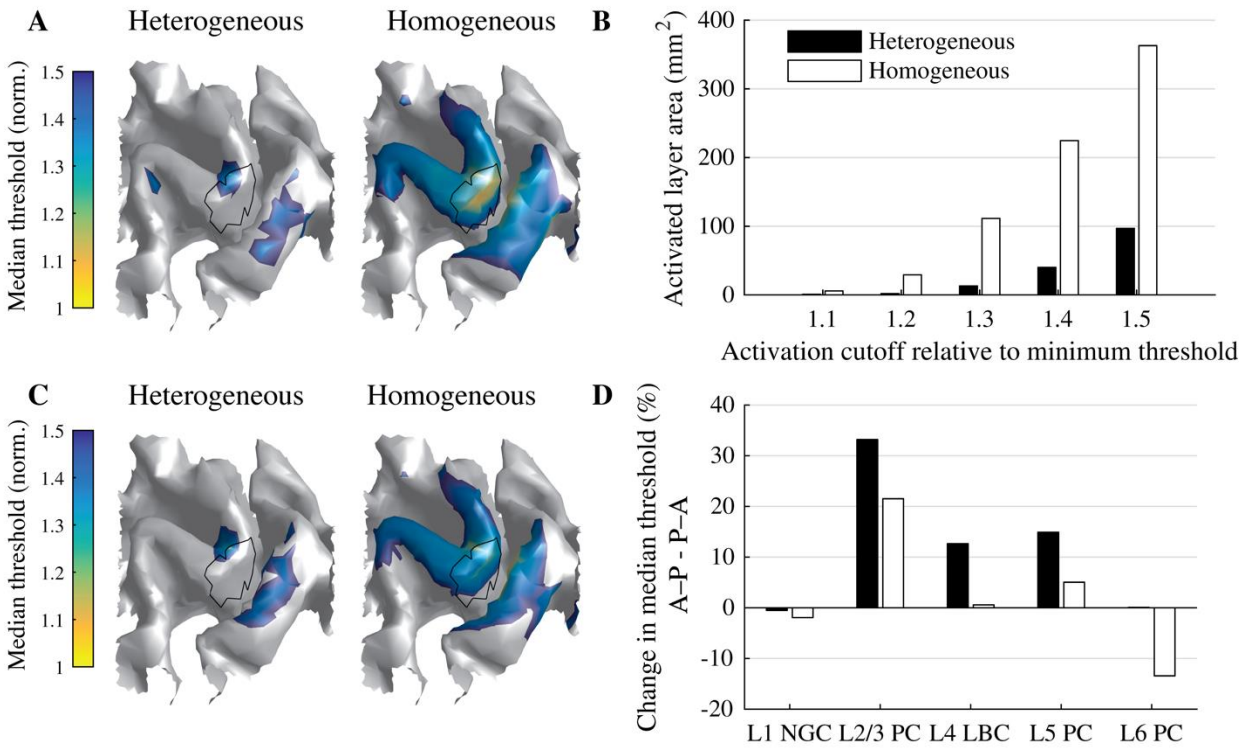


**Supplementary Figure 6. Homogeneous intracranial conductivity reduces the focality of neural activation and alters the effect of current direction. A)** Median thresholds (across 5 clones and 6 rotations) for L5 PCs with heterogeneous and homogeneous intracranial conductivities in the FEM for monophasic P–A stimulation with MagVenture MC-B70 coil. Thresholds are normalized to individual minima (77.6 A/µs for heterogeneous case; 122.4 A/µs for homogeneous case) and color map is limited to 1.5 times this value to indicate relative spread of activation. **B)** Focality of L5 activation quantified as surface area with thresholds below a certain cutoff relative to the minimum threshold. Cutoffs were set to 1–1.5 times the threshold minimum for the heterogeneous or homogeneous case, respectively. **C)** Same as A for monophasic A–P stimulation. **D)** Change in median threshold of L5 PCs within hand muscle representation (outlined in A and C, same as in Figure 6) comparing A–P versus P–A stimulation.

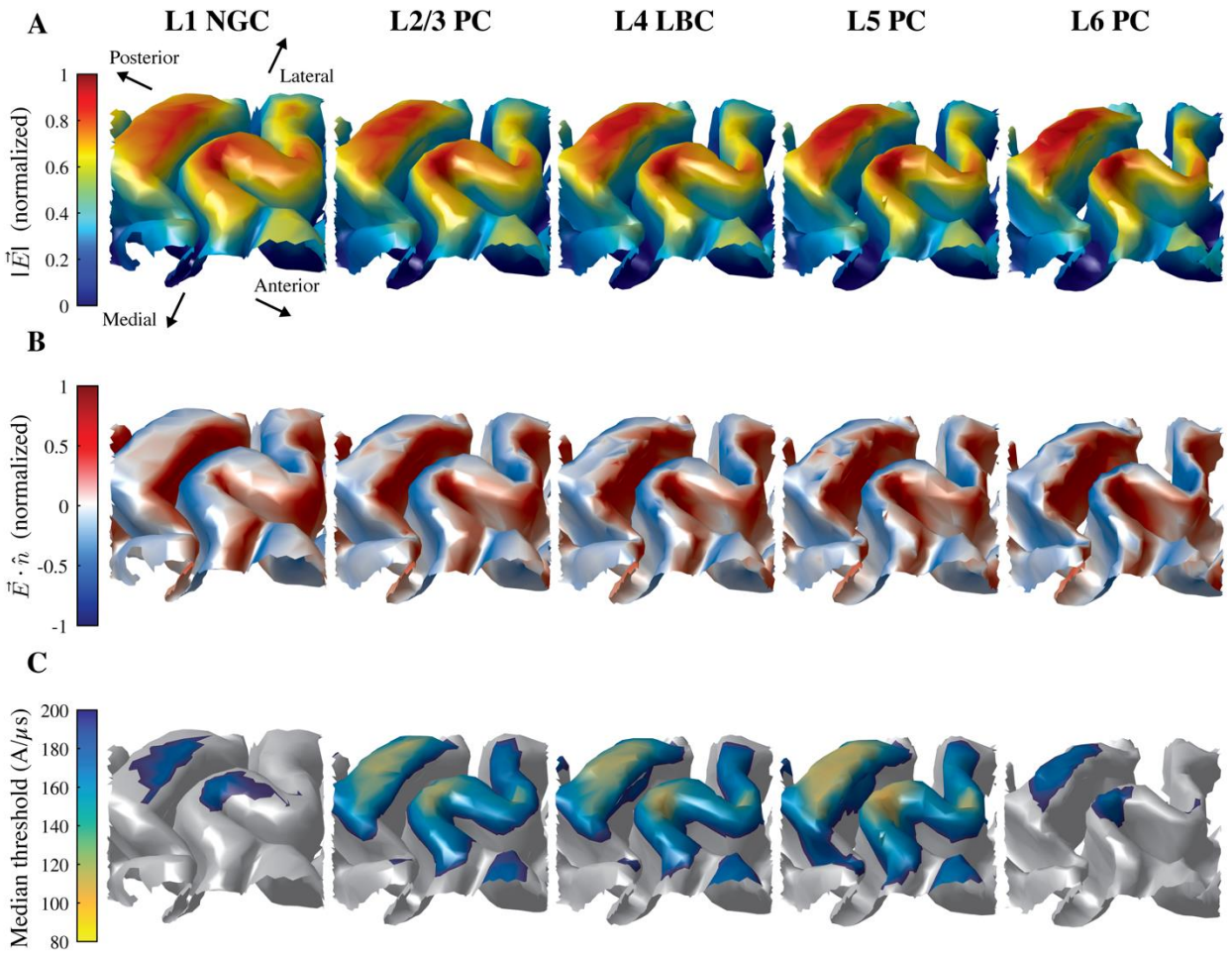


**Supplementary Figure 7. Low threshold region extends further into posterior wall of central sulcus than anterior wall.** Low threshold region extends further into posterior wall of central sulcus than anterior wall. Alternative view of plots in Figure 3 from anterior side (facing posterior) of **A)** magnitude of simulated E-field (normalized to maximum layer) on layer surfaces for L1–L6, **B)** component of E-field normal to layer surfaces (normalized to maximum layer), and **C)** median thresholds (across 5 clones and 6 azimuthal rotations) for monophasic P–A simulation.

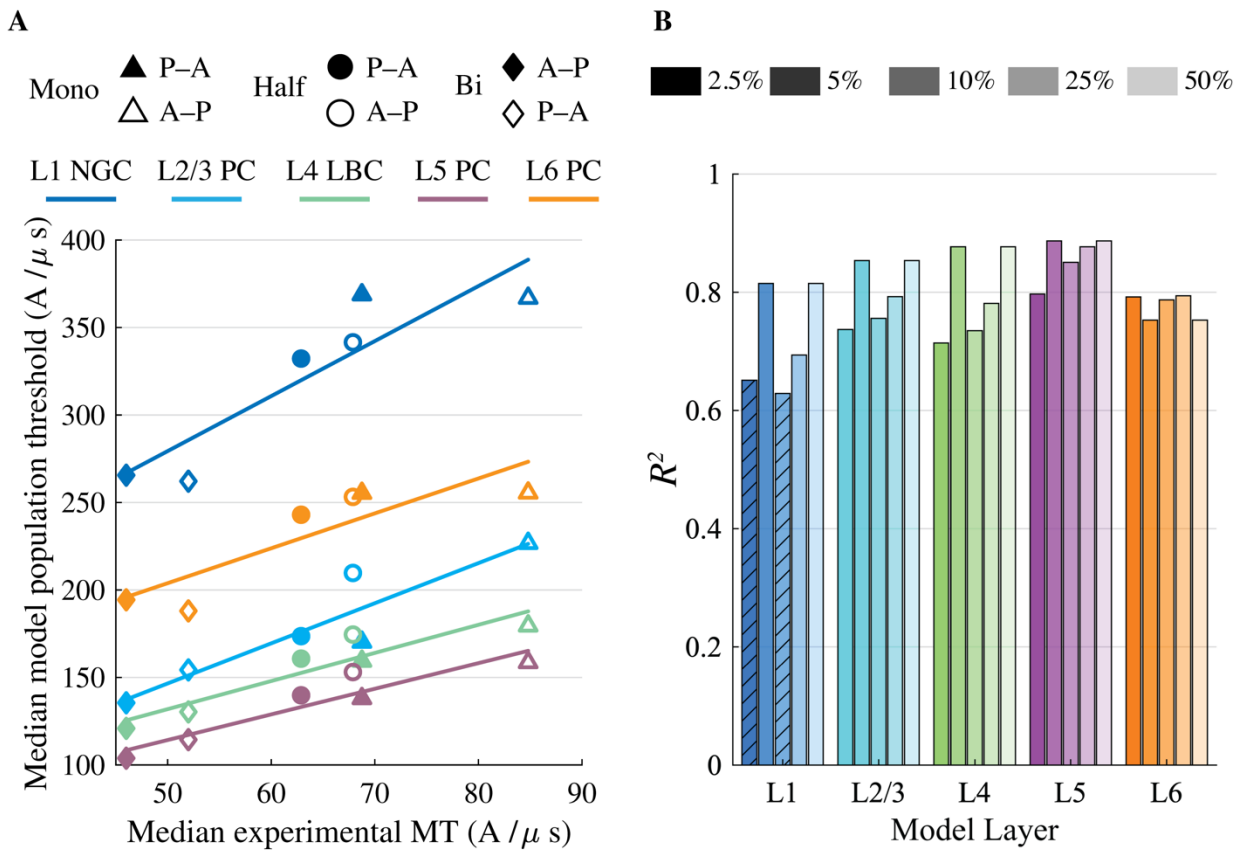


**Supplementary Figure 8. Model population thresholds correlate with experimental motor thresholds across pulse waveforms and directions. A)** Median model population thresholds within hand muscle representation in each layer (same as Figure 6) plotted against median experimental motor thresholds for 12 subjects [37]. Linear regression for each layer included as solid line. **B)** Coefficients of determination for linear correlations of model population thresholds for threshold percentiles of 2.5–50% within the hand muscle representation and the median experimental motor thresholds [36]. Boxes that are not hashed indicate statistically significant correlation ($p < 0.05$).

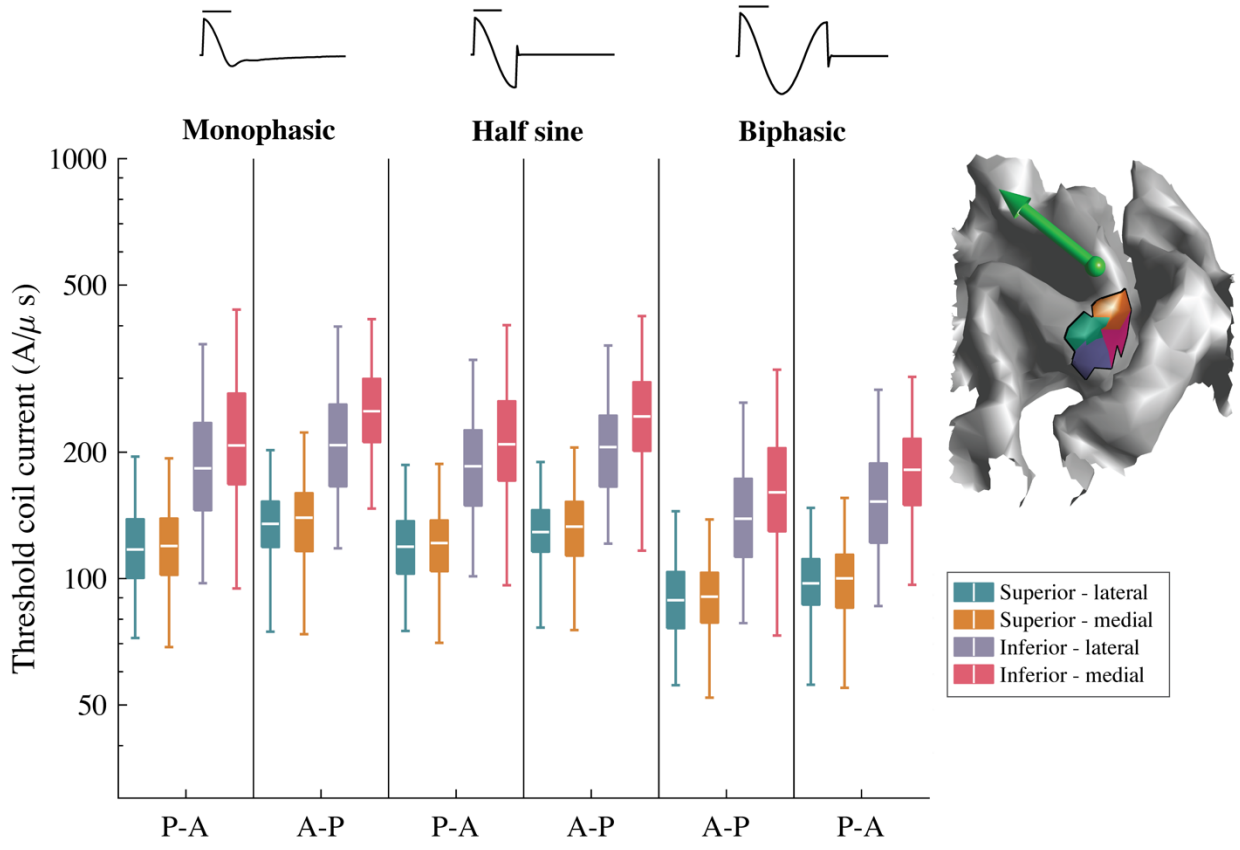


**Supplementary Figure 9. Activation thresholds of L5 PCs within sub-regions of putative hand muscle representation.** Each boxplot describes statistics (same as Figure 6) of thresholds from 5 clones and 6 rotations of L5 PCs at each position within a color-coded sub-region of the putative hand muscle representation on the L5 surface (black outline, right; same as in Figure 6). Green arrow indicates center of TMS coil and direction of induced current (for P–A stimulation).

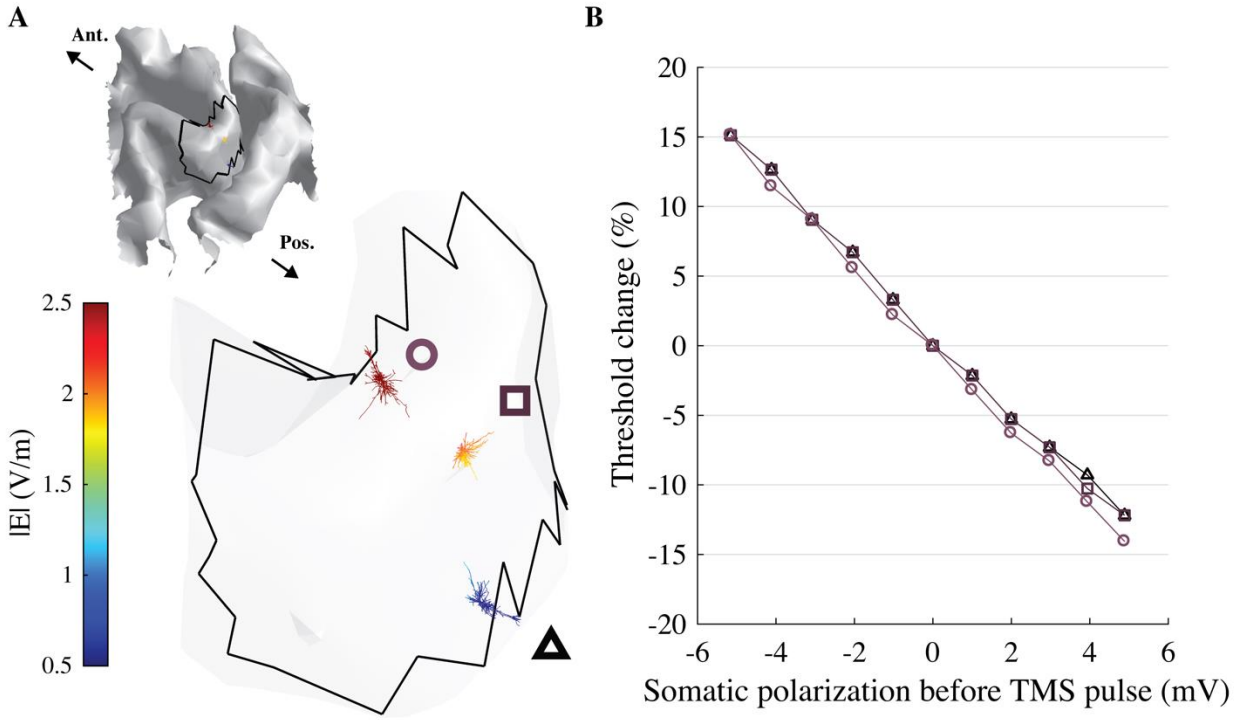


**Supplementary Figure 10. Effect of subthreshold polarization on TMS activation thresholds for example L5 PCs.** The effect of steady-state, subthreshold polarization on TMS thresholds was simulated in three example L5 PCs within the motor hand knob by determining activation thresholds for monophasic P–A TMS after 150 ms of dc current injection to the proximal apical trunk. The amplitude of current injection was controlled by first determining the polarization per nA for 150 ms of current injection, which was then used to estimate the current amplitude necessary to produce somatic polarization between −5 mV and 5 mV. The neurons were coupled to the local E-field induced by the MagVenture MC-B70 coil, as described in the main text. Thresholds to elicit a single action potential were then determined for a TMS pulse applied at 150 ms during a simulation of 152 ms total duration (ending 2 ms after the TMS pulse) using a binary search algorithm with a 5 μs time step. Panel description: **A)** Model neuron morphologies of three representative L5 PCs in gyral crown (circle), lip (square), and upper sulcal wall (triangle) of motor hand knob, shown embedded in semi-transparent L5 surface (close-up of same gyrus shown in Figure 2B). Full L5 surface shown in top inset. Morphologies colored with E-field magnitude at each compartment for E-field induced by MagVenture MC-B70 coil. **B)** Change in threshold relative to no current injection for monophasic P–A TMS as pre-stimulation somatic polarization is varied. Each curve corresponds to the L5 PC with the same symbol as in A. The threshold changes were mediated through axonal polarization, as somatic polarization caused passive polarization of the axon, bringing the activated neuronal elements closer or farther from threshold in an essentially linear fashion.